Available online at www.sciencedirect.com
ScienceDirect
Ceramics International 35 (2009) 3275–3280
CERAMICS INTERNATIONAL
www.elsevier.com/locate/ceramint

# Preparation of $TiO_2$ nanofilm via sol–gel process and its photocatalytic activity for degradation of methyl orange

Lijuan Chen, Jintao Tian *, Huang Qiu, Yansheng Yin, Xin Wang, Jinhui Dai, Pingwei Wu, Aiping Wang, Lei Chu

*Institute of Materials Science and Engineering, Ocean University of China, Songling Road 238, Qingdao 266100, PR China*

Received 19 March 2009; received in revised form 2 April 2009; accepted 22 May 2009
Available online 18 June 2009

**Abstract**

The preparation of $TiO_2$ nanofilm was conducted on common glass via the sol–gel process. Glacial acetic acid and diethanolamine were used as inhibitors to prepare acidic and alkaline $TiO_2$ sol, respectively. XRD, SEM, and EDS characterization showed that the film prepared from acidic $TiO_2$ sol had a narrow particle size distribution of ~15–30 nm and relatively poor particle crystallization while in the case of the film from alkaline $TiO_2$ sol the nanoparticles were in a wide range of ~10–80 nm and well crystallized. The photolysis evaluation through MO degradation revealed that the film from acidic sol possessed apparently better photocatalytic activity than that from alkaline sol. Heat treatment with longer time led to a ~50% increase of the photocatalytic activity for the film.


*Keywords:* D. $TiO_2$; Thin film; Sol–gel growth; Photolysis

## 1. Introduction

With high surface activity, strong catalyzing ability, and high chemical stability, titanium dioxide ($TiO_2$) has attracted a great deal of attention as photocatalyst for environmental purification [1–5]. Contrary to $TiO_2$ powder, $TiO_2$ film does not create conglomeration and can be easily reclaimed after reaction. In particular, $TiO_2$ film has higher surface activity, endowing the material with a wide industrial application for antibacterial and self-cleaning [6–9]. $TiO_2$ film can be prepared via several methods such as chemical vapor deposition [10], hydrolysis deposition [11], chemical spray pyrolysis [12], pulsed laser deposition [13], and sol–gel method [14]. In comparison with other methods, sol–gel process has notable advantages such as high purity, good uniformity of the film microstructure, low temperature synthesis, easily controlled reaction condition, and therefore has been frequently adopted to prepare the nano-structured $TiO_2$ film [15].

Although up to now large amount of studies have been focused on $TiO_2$ film described above, some unexploration remains. There is still not much known about the film preparation and its performance. For instance, the film can be prepared via sol–gel process from either acidic sol or alkaline sol, probably a key condition that might affect the film characteristic and therefore performance to some extent. In this study we would like to focus our attention on this. The $TiO_2$ film was prepared via sol–gel process from acidic and alkaline $TiO_2$ sol using glacial acetic acid and diethanolamine as inhibitors, respectively. The so-prepared film after heat treatment was characterized using XRD, SEM, and EDS. The photocatalytic efficiency of the film was evaluated via photodegradation of methyl orange (MO) solution under UV irradiation.

## 2. Experimental procedure

### 2.1. Preparation and characterization of the $TiO_2$ nanofilm

In the present study the $TiO_2$ nanofilm was prepared via sol–gel process using common glass as substrate. Titanium tetrabutylate (Aldrich, 99.99%, TTB) was used as a precursor to prepare $TiO_2$ sol at room temperature. Firstly the TTB was dissolved in ethanol and stirred for half an hour to get a precursor solution. A mixture of distilled water, glacial acetic

* Corresponding author. Tel.: +86 532 66781690; fax: +86 532 66781320.
*E-mail address:* jttian@ouc.edu.cn (J. Tian).

0272-8842/$36.00 
doi:10.1016/j.ceramint.2009.05.021

acid, and ethanol was then dropped into the precursor solution at a speed of one drop per second under a strong stirring. After that, the solution was continuously stirred for 1 h to achieve a yellow transparent sol. The sol was then aged for a period of time. Here the glacial acetic acid was used as an inhibitor to slow down the TTB fast hydrolysis. In this case the pH value of the system was measured to be ~5, and the obtained $TiO_2$ sol was hereafter referred to be as acidic sol. On the other hand, another inhibitor of diethanolamine (Aldrich, 99.99%, DEA) was used and the pH value of the system was determined to be ~10. The prepared $TiO_2$ sol in this case was hereafter referred to be as alkaline sol.

The $TiO_2$ nanofilm was prepared by depositing the $TiO_2$ sol on substrate glass via dip-coating method at room temperature. Prior to the coating process, the glass was washed several times with water, ultrasonically cleaned in ethanol for 20 min, and in acetone for 20 min, respectively. The cleaned glass was then immersed into the $TiO_2$ sol and withdrawn at a speed of 2 mm/s. In this way the substrate glass was covered with a thin layer of the nano-$TiO_2$ particle. The uniform film was naturally dried in air and the coating operation was repeated again. The coated specimen was then heat treated at 100 °C for 1 h and at 500 °C for 2 h. The temperature increase during the heating process was kept at a speed of 1 °C/min. After heat treatment, the specimen was naturally cooled.

The so-prepared $TiO_2$ nanofilm was characterized as below. The crystalline phase of the film was identified through X-ray diffraction (XRD) method. The microstructural morphology of the film was observed using scanning electron microscopy (SEM). The elemental analysis of the film was performed using energy dispersive spectroscopy (EDS).

### 2.2. Evaluation of photocatalytic activity of the $TiO_2$ nanofilm

The photocatalytic activity of the $TiO_2$ nanofilm prepared in this study was assessed from the kinetics of the decomposition of methyl orange (MO) solution using the film as photocatalyst under UV irradiation. As the photodegradation of MO solution catalyzed by $TiO_2$ can be well governed by the Langmuir–Hinshelwood model [16,17], the reaction rate can be expressed as

$$-\ln\left(\frac{C}{C_0}\right) = K_t \quad (1)$$

where $C$ is the concentration of MO solution at time $t$ = t, $C_0$ is the concentration at time $t = 0$, $K$ is the apparent reaction rate constant, and $t$ is the reaction time. A plot of $-\ln(C/C_0)$ versus $t$ will yield a slope of $K$. By comparing the $K$ value the evaluation of the photocatalytic activity of the film was achieved.

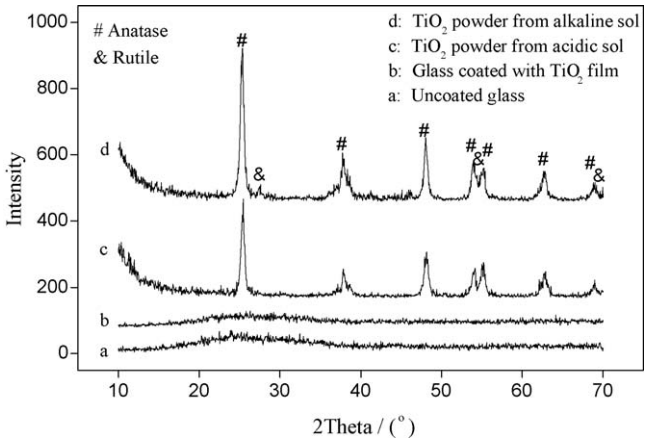


Fig. 1. XRD patterns of the $TiO_2$ nanofilm and $TiO_2$ powder after a 500 °C heat treatment for 2 h.

The experimental photodegradation of MO solution in this study was carried out as below. A MO solution with a certain concentration was prepared as an initial solution. The $TiO_2$ film was immersed into a small beaker filled with some amount of the initial MO solution. The reaction system was then illuminated using a 20 W UV lamp for a period of time. After reaction, the concentration of the MO solution was determined by measuring the absorbance at 465 nm using a UV–vis spectrophotometer.

## 3. Results and discussion

### 3.1. Crystallization of the $TiO_2$ nanofilm

The $TiO_2$ nanofilm was prepared via sol–gel process from a $TiO_2$ sol followed by heat treatment at high temperature. In order to identify the phase composition of the film, the XRD measurement was conducted on the coated substrate and the result was shown in Fig. 1. Besides this, the XRD measurement on the uncoated glass was also performed and the result was incorporated in this figure for comparison. As seen from Fig. 1a and b, no intensive peak was observed in the XRD patterns, indicating an amorphous state of the coated specimen. This was probably due to the fact that the film was too thin to be detected out during the XRD measurement. So the $TiO_2$ sol was gelled and heat treated to be $TiO_2$ powder under a heating process absolutely identical to that used for the film. The XRD measurement on this powder was conducted and the result was shown in Fig. 1c and d. For quantitative purpose, the average

Table 1
Average particle size $D_c$ (nm) of the $TiO_2$ nanofilm from XRD and SEM.

| Time for heat treatment | $TiO_2$ nanofilm | $D_c$ from XRD | | | Crystallinity degree | $D_c$ from SEM |
|---|---|---|---|---|---|---|
| | | FWHM | $2\theta$ | $D_c$ | | |
| 2 h | From acidic sol | 0.504 | 25.4 | 16.0 | ~70% | ~15–30 |
| 2 h | From alkaline sol | 0.517 | 25.3 | 15.6 | ~80% | ~10–80 |

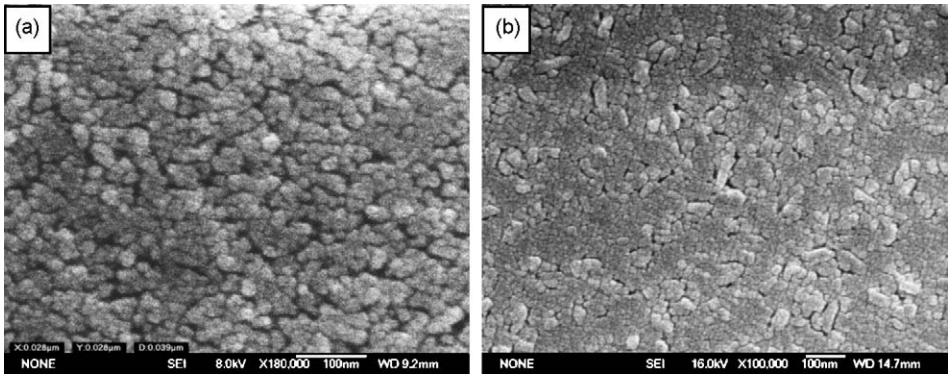


Fig. 2. SEM morphology of the $TiO_2$ nanofilm prepared from acidic sol (a) and alkaline sol (b).

particle size $D_c$ of crystallites in the film was also estimated from the peak half-width $B$ using the Sherrer equation [18]:

$$D_c = \frac{k\lambda}{(B\cos\theta)} \quad (2)$$

where $k$ is a shape factor of particles (normally chosen as 0.89), $\lambda$ is the wavelength of X-ray in nanometer (0.1541 nm for Cu K$\alpha$ in this study), and $\theta$ is the incident angle of X-ray, respectively. The calculated results are shown in Table 1.

As seen from Fig. 1c and d, crystallized pure $TiO_2$ of anatase after a 500 °C heat treatment for 2 h was obtained. The sharp peaks revealed a good crystallization of the $TiO_2$ nanoparticles under such condition. The calculated average particle size $D_c$ from Sherrer equation, as shown in Table 1, was comparative to each other in nanoscale and comparable to those estimated from SEM observations. One interesting point in this figure was that the diffraction peak intensities in Fig. 1d was evidently higher than those in Fig. 1c, indicating better crystallization of $TiO_2$ powder from alkaline sol than that from acidic sol. In fact, trace amount of rutile, a phase of $TiO_2$ normally formed at higher temperature, has been observed in Fig. 1d. The roughly estimated crystallinity degree was ~70% and ~80%, respectively (see data in Table 1), showing a noticeable difference of crystallinity for the two powders. Such results suggested that the crystallization behavior of the $TiO_2$ particles was apparently varying with the application of inhibitors.

### 3.2. Microstructural morphology of the $TiO_2$ nanofilm

The SEM observation of the $TiO_2$ nanofilm was performed and the results are shown in Fig. 2. As seen from Fig. 2, the $TiO_2$ film from acidic sol was composed of nanoparticles with a narrow particle size range of ~15–30 nm (Fig. 2a). All the nanoparticles are uniformly distributed in the film. The cross-sectional SEM view of the film revealed a film thickness of ~250 nm. This was in good agreement with the XRD measurement, where the film was presumed to be rather thin. The $TiO_2$ film from alkaline sol also consisted of nanoparticles. The particle size in this case, however, was in a rather wide range of ~10–80 nm (Fig. 2b), leading to a microstructural morphology of the film visibly different from that shown in Fig. 2a. Thus, it was suggested that the microstructural morphology of the $TiO_2$ nanofilm clearly altered with the application of inhibitors.

In order to identify the element composition of the $TiO_2$ nanofilm, the EDS analysis was conducted on the surface of the film during the SEM observation. The results are shown in Fig. 3. Elements of oxygen (O), silicon (Is), sodium (Na), calcium (Ca), etc., were detected to be present on the surface of the specimen. These elements were from the substrate glass, a sign of the film being rather thin. The platinum (Pt) was from the platinum coating for electron conductivity. Element of Ti was found present and distributed homogeneously in the film, indicating successful preparation of the $TiO_2$ film in this study.

### 3.3. Photocatalytic activity of the $TiO_2$ nanofilm

The photocatalytic activity of the $TiO_2$ nanofilm was assessed from the kinetics of photodegradation of MO solution. In this case the film thickness was estimated to be ~500 nm. The initial concentration of MO solution and the maximum reaction time for photodegradation was firstly experimentally determined from Fig. 4. In comparison with that of 0.05 mmol/l, by using the MO solution with an initial concentration of 0.025 mmol/l a sharp decrease of the UV–vis absorption was observed, as shown in Fig. 4a. Thus, the MO solution with initial concentration of 0.025 mmol/l was adopted for subsequent photodegradation. By using the catalyst of the $TiO_2$ nanofilm under UV irradiation, the MO solution was photodecomposed to be nearly transparent after 7 h (Fig. 4b).

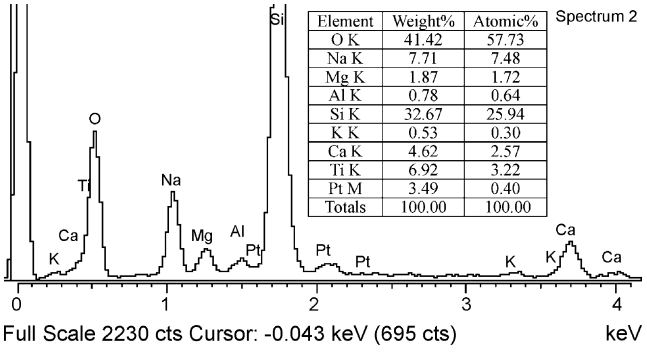


Fig. 3. EDS analysis of element composition of the $TiO_2$ nanofilm.

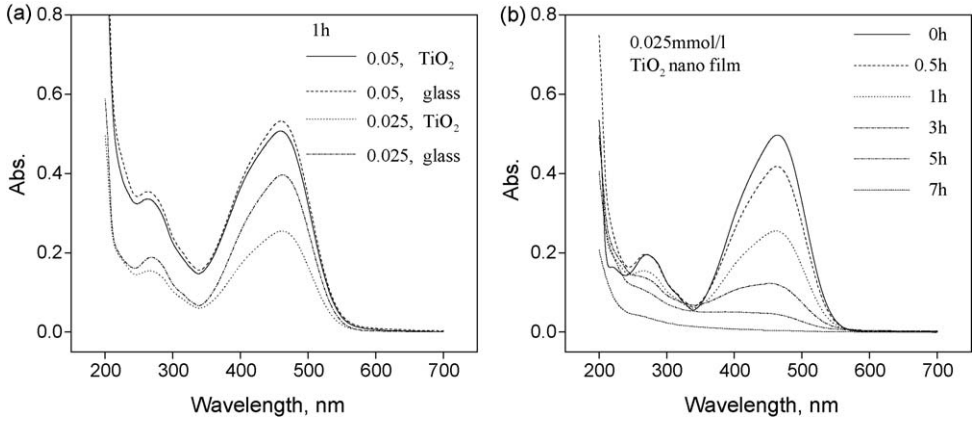


Fig. 4. UV–vis absorption spectra of MO solution catalyzed by the $TiO_2$ nanofilm under UV irradiation. These experiments were applied to determine the initial concentration of MO solution and the maximum reaction time, respectively.

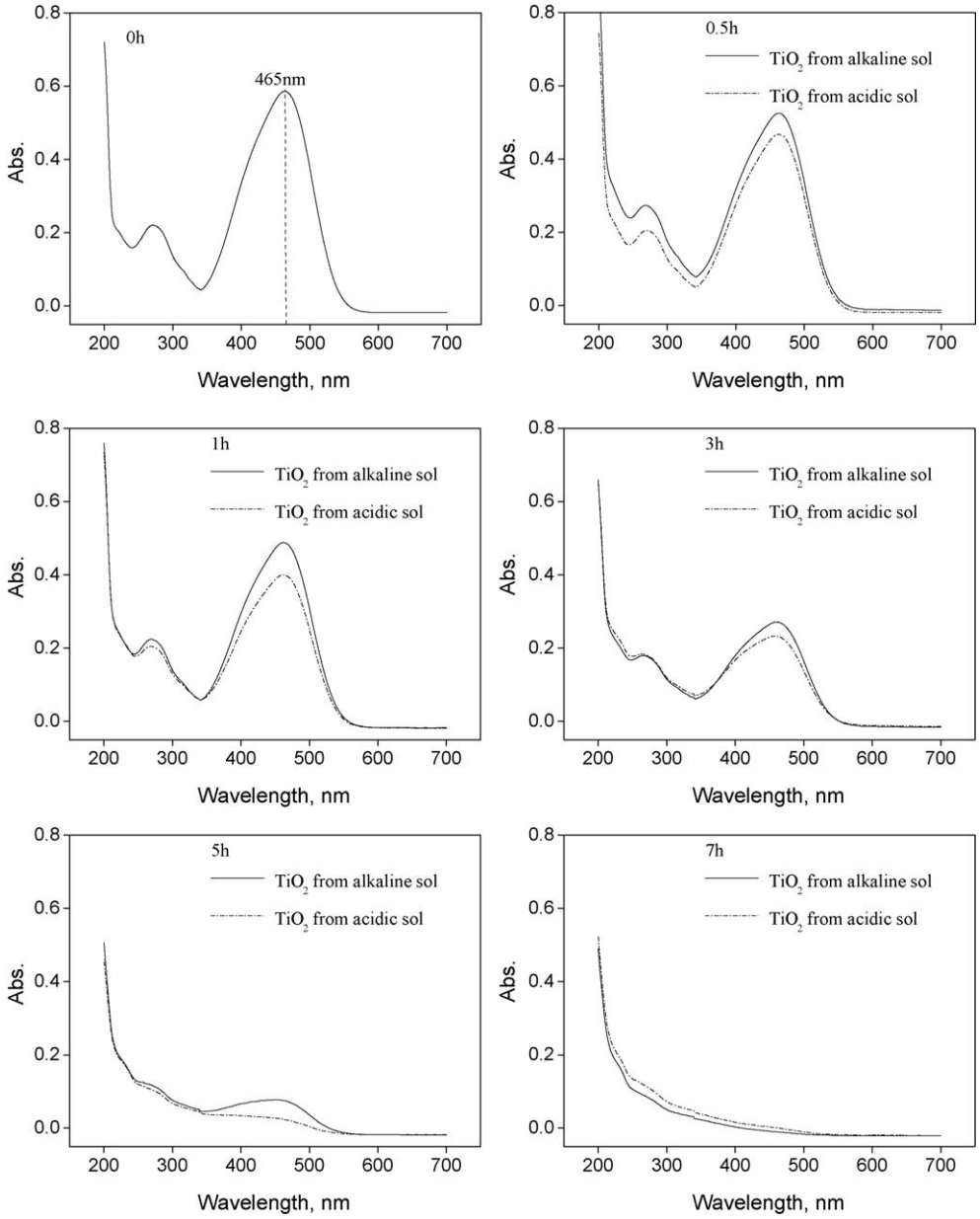


Fig. 5. UV–vis absorption spectra of MO solution catalyzed by the $TiO_2$ nanofilm under UV irradiation.

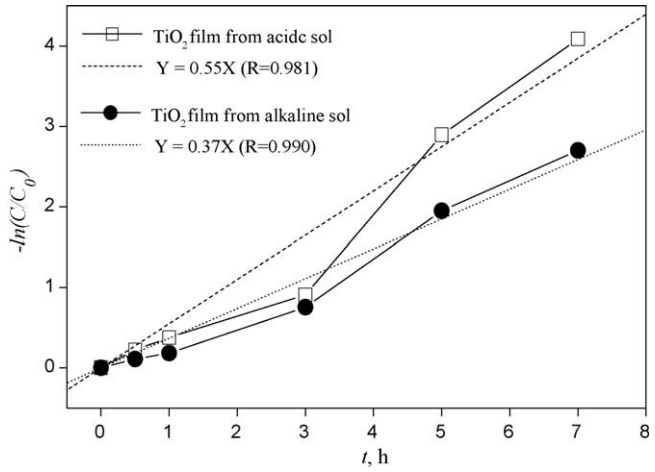


Fig. 6. Relationship between $-\ln(C/C_0)$ and reaction time $t$ for MO decomposition catalyzed by the $TiO_2$ nanofilm under UV irradiation.

Table 2
Apparent reaction rate constant $k$ ($h^{-1}$) of MO decomposition catalyzed by the $TiO_2$ nanofilm under UV irradiation.

| Time for heat treatment | $TiO_2$ nanofilm | $-\ln(C/C_0) = kt$ | |
|---|---|---|---|
| | | $k$ | $R$ |
| 2 h | From alkaline sol | 0.37 | 0.990 |
| 2 h | From acidic sol | 0.55 | 0.981 |
| 5 h | From acidic sol | 0.40 | 0.996 |
| 10 h | From acidic sol | 0.60 | 0.982 |

Accordingly, a maximum reaction time of 7 h was applied in this study.

The photodegradation of MO solution was conducted using the $TiO_2$ nanofilm as catalyst under UV irradiation. The reaction time was scheduled to be 0 h, 0.5 h, 1 h, 3 h, 5 h, and 7 h. The resultant UV–vis absorption spectra are shown in Fig. 5. All the spectra in Fig. 5 displayed maximum UV–vis absorptions at wavelength of 465 nm, a sign of MO concentration level after degradation. As seen, the MO solution catalyzed by the $TiO_2$ nanofilm from acidic sol shows maximum absorption values at 465 nm evidently lower than those catalyzed by the film from alkaline sol. This indicated that the $TiO_2$ film from acidic sol had higher photocatalytic activity than the film from alkaline sol.

The quantitative determination of photocatalytic activity for the $TiO_2$ nanofilm was achieved as below. As it is well accepted that the photodegradation of MO solution accords with a pseudo first-order kinetic [16,17], the relationships between $-\ln(C/C_0)$ and reaction time $t$ were plotted and shown in Fig. 6. The derived apparent reaction rate constant $k$ was summarized in Table 2. As seen from Fig. 6 and Table 2, the $k$ value for the $TiO_2$ film from acidic sol was apparently larger than that for the film from alkaline sol. Thus, it was concluded that the $TiO_2$ film from acidic sol possessed higher photocatalytic activity than the film from alkaline sol.

### 3.4. Effect of heat treatment time on the photocatalytic activity of the film

Besides the microstructural morphology shown in Fig. 2, the particle crystallization was also clearly varying with the application of inhibitors, as shown in Fig. 1. The $TiO_2$ film from acidic sol possessed higher photocatalytic activity but lower crystallinity degree. Thus, it was expected to enhance film crystallization and therefore improvement of photocatalytic activity for the film. For such purpose the film was heat treated with longer time of 5 h and 10 h, respectively, and its photocatalytic activity was assessed. The results are shown in Fig. 7. The maximum values of UV–vis absorption in Fig. 7 for the film with 10 h heat treatment were visibly lower than those for the film with 5 h heat treatment. The plot of $-\ln(C/C_0)$ versus reaction time $t$ in Fig. 8 revealed apparently improvement of the $k$ value. An increase of ~50% in this case was achieved for the $k$ value, indicating a substantial improvement of the photocatalytic activity of the film due to the longer time heat treatment. Fig. 9 showed the XRD measurements of the film with different heat treatment times. For 5 h heat treatment better crystallization was achieved. With time longer than 5 h, for instance 10 h, the peak intensities in this figure, however, were not visibly increased. Such results indicated that the effect of the heat treatment time on the photocatalytic activity of the $TiO_2$ nanofilm was quite complicated. It was presumed that not only the particle crystallization but also the particle micro-

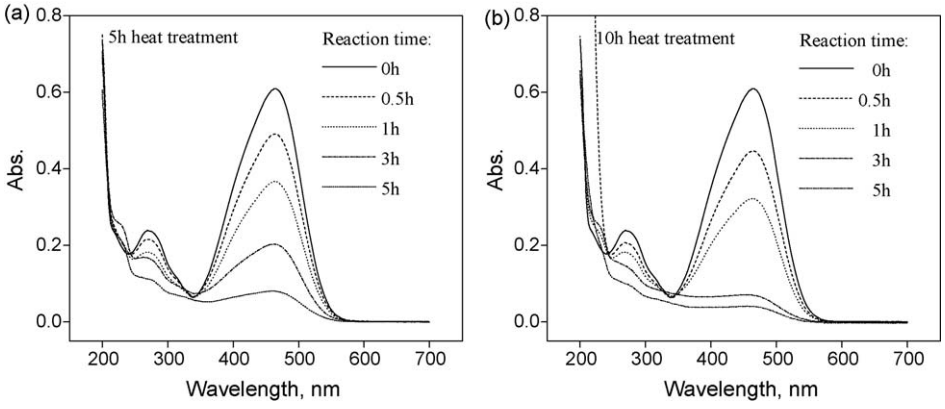


Fig. 7. UV–vis absorption spectra of MO solution catalyzed by the $TiO_2$ nanofilm under UV irradiation. The film was heat treated for 5 h and 10 h, respectively.

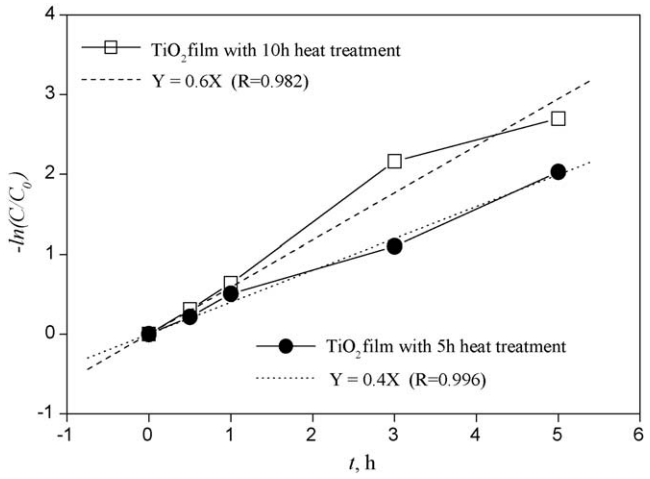


Fig. 8. Relationship between $-\ln(C/C_0)$ and reaction time $t$ for MO decomposition catalyzed by the $TiO_2$ nanofilm under UV irradiation. The film was heat treated for 5 h and 10 h, respectively.

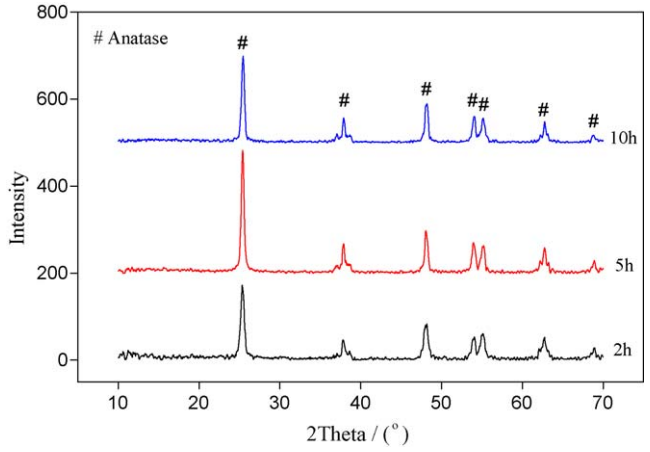


Fig. 9. XRD patterns of the $TiO_2$ powder from acidic sol after a 500 °C heat treatment for 2 h, 5 h, and 10 h, respectively.

structural evolution during the heating process could affect the film performance to some extent.

## 4. Conclusion

In the present study the $TiO_2$ nanofilm was prepared via sol–gel process using common glass as substrate. In order to slow down the fast hydrolysis of the titanium tetrabutylate, inhibitors of glacial acetic acid and diethanolamine were used to prepare acidic and alkaline $TiO_2$ sol, respectively. The film characterization through XRD, SEM, and EDS indicated that the film prepared from acidic $TiO_2$ sol had a narrow particle size distribution of ∼15–30 nm and relatively poor particle crystallization while in the case of the film from alkaline $TiO_2$ sol the nanoparticles were in a wide range of ∼10–80 nm and well crystallized. The photolysis evaluation through MO degradation revealed that the film from acidic sol possessed apparently better photocatalytic activity than that from alkaline sol. Heat treatment with longer time led to a ∼50% increase of the photocatalytic activity for the film. The XRD measurements, however, revealed a quite complicated mechanism where not only particle crystallinity degree but also particle morphology evolution during the heating process should be considered.

## Acknowledgements

This work was financially supported by Doctoral Program Foundation of Institutions of Higher Education of China (200804231004) and Ocean University of China-Student Research Training Program (OUC-SRTP, 0811011707).

## References

[1] M.S. Ghamsari, A.R. Bahramian, Mater. Lett. 62 (2008) 361.
[2] D.W. Kim, S. Lee, H.S. Jung, Int. J. Hydrogen Energy 32 (2007) 3137.
[3] R.M. Alberici, W.F. Jardim, Appl. Catal. B: Environ. 14 (1997) 55.
[4] K. Wang, J. Jehng, Y. Hsieh, J. Hazard. Mater. B90 (2002) 63.
[5] M.L. Sauer, D.F. Ollis, J. Mater. Sci. 36 (2001) 5923.
[6] N.P. Mellott, C. Durucan, C.G. Pantano, M. Guglielmi, Thin Solid Films 502 (2006) 112.
[7] T. Watanabe, A. Nakajima, R. Wang, M. Minabe, S. Koizumi, A. Fujishima, K. Hashimoto, Thin Solid Films 351 (1999) 260.
[8] V. Roméas, P. Pichat, C. Guillard, T. Chopin, C. Lehaut, Ind. Eng. Chem. Res. 38 (1999) 3878.
[9] K. Guan, Surf. Coat. Technol. 191 (2005) 155.
[10] A. Aidla, T. Uustare, A.A. Kiisler, J. Aarik, V. Sammelselg, Thin Solid Films 305 (1997) 270.
[11] Y. Shi, G. Xie, Electric Machine & Electric Apparatus Technologies, vol. 3, 2000, p. 37 (in Chinese).
[12] M.O. Abou-Helal, W.T. Seeber, Appl. Surf. Sci. 195 (2002) 53.
[13] Y. Choi, S. Yamamoto, T. Umebayashi, M. Yoshikawa, Solid State Ionics 172 (2004) 105.
[14] L. Hu, T. Yoko, H. Kozuka, Thin Solid Films 219 (1992) 18.
[15] P. Chrysicopoulou, D. Davazoglou, Chr. Trapalis, G. Kordas, Thin Solid Films 323 (1998) 188.
[16] Y.J. Li, X.D. Li, J.W. Li, J. Yin, Water Res. 40 (2006) 1119.
[17] J. Matos, J. Laine, J.M. Hermann, Appl. Catal. B: Environ. 18 (1998) 281.
[18] A.L. Patterson, Phys. Rev. 56 (1939) 978.